Composites & nanocomposites

Mechanical properties and conductivity of graphene/Al-8030 composites with directional distribution of graphene

YuMing Guo[1,2] (ID), DanQing Yi[1,2,*], HuiQun Liu[1,2], Bin Wang[1,2], Bo Jiang[1,2], and HaiSheng Wang[1,2,3]

[1] School of Materials Science and Engineering, Central South University, Changsha 410083, China

[2] Key Laboratory for Nonferrous Materials Science and Engineering, Education Ministry, Central South University, Changsha 410083, China

[3] Department of Mechanical Engineering, Honghe University, Mengzi 661100, China

ABSTRACT

Composites of graphene nanoplatelets (GNPs) and 8030 aluminum alloy powder were prepared using powder modification + semisolid extrusion processes. The density, electrical conductivity, mechanical properties and microstructure of the specimens were investigated. The results show that the composites with 0.5 wt% GNPs achieved an enhancement in yield strength (37.5%) and ultimate tensile strength (62.9%), while its elongation and electrical conductivity were comparable, as compared with the 8030 aluminum alloy without GNPs prepared by the same process. Furthermore, the related strengthening mechanism of the composites with GNPs directional distribution was discussed.

Introduction

8030 aluminum alloy (Al-8030) is a kind of Al–Fe–X series cable core material for construction industry. It has good creep resistance and high electrical conductivity, but the disadvantage of lower mechanical strength limits its application [1, 2]. It is difficult to obtain satisfactory comprehensive performance of Al-8030 by adding alloying elements. For example, in the previous research work of our group, the rare earth element Sc and trace Cu were added to the Al-8030 alloy to achieve effective enhancement of tensile strength, but the plasticity and electrical conductivity of the alloy were also found to be largely reduced [3, 4]. Since the added alloying elements tend to form hard and brittle intermetallic compounds with the matrix, the conductivity of these compounds is poor.

It may be an effective breakthrough to change a tough and electrically conductive reinforcement. In recent years, graphene has become a research hotspot due to its large specific surface area, high mechanical properties [5], Young's modulus [6], electrical [7] and thermal conductivity [8], etc., which let it to be used as a good reinforcement for alloy. Numerous studies have reported that the strength of alloy matrix can be improved by adding graphene [9–14]. However, we

Table 1 Chemical compositions of the as-atomized Al-8030 powders

Materials	Composition (wt%)						
	Al	Fe	Cu	Si	Mg	Zn	B
Standard of ASTM-B800-05	Bal.	0.3–0.8	0.15–0.3	0.1	0.05	0.05	0.001–0.04
Al-8030 powder	Bal.	0.67	0.25	0.047	0.001	0.001	0.001

can also find that the distribution of graphene in the composites is random, which weakens the reinforcing effect of graphene. The research results of Li et al. [15] showed that the influence of graphene in the composites on the electrical conductivity was mainly caused by the blocking of moving electrons by the phase interface. Adjusting the distribution direction of graphene is consistent, which can improve the reinforcing effect of graphene and minimize the scattering of electrons by graphene in the distribution direction. Therefore, it is expected to improve the comprehensive performance of the Al-8030 alloy by adding graphene and orienting the graphene in the alloy. Until now, there have been few reports on this aspect.

The orientation distribution of graphene in the alloy can be achieved by the preparation process. In most cases, traditional powder metallurgy method has been used for the preparation of graphene-reinforced metal matrix composites [11, 16, 17]. However, the structure of graphene is easily destroyed during ball milling and secondary molding processes [10, 16, 18, 19]. In the present study, powder-modified + ball-free wet mixing process is used and then formed by a semisolid extrusion process. This process fully protects the graphene structure from being destroyed during the preparation process, and at the same time, the semisolid metal and graphene has better wettability under the pressing force to obtain a high-density sample. Most importantly, this process helps to obtain an oriented arrangement of graphene in the metal matrix through the coordinated deformation of graphene and semisolid metal powder during the extrusion process.

Experimental

Materials

The graphene nanoplatelets (GNPs) with a lateral size of 8.96 μm and atomized Al-8030 powder (99.9% in purity) were used in this work. According to

previous research reports [9, 10, 16, 20], when the GNPs content is > 1.0 wt% or < 0.3 wt%, the enhancement effect of the composites is not satisfactory. Therefore, the addition of GNPs in this experiment is 0.5 wt%. The chemical composition of Al-8030 powder is listed in Table 1, from which it can be seen that the content of all elements conforms to the ASTM-B800-05 standard.

Experimental procedures

In order to determine the suitable temperature for the semisolid extrusion, the ratio of solid–liquid phase in the semisolid range of Al–0.7Fe–0.25Cu (close to the composition of Al-8030) was calculated by Thermo-Calc software (Fig. 1a). At the same time, the DTA test was performed on the Al-8030 powder. In the DTA graph in Fig. 1b, it can be seen that the liquid phase appears initially at about 640 °C, and its mass fraction reaches the maximum at 664 °C, indicating that Al-8030 will be completely melted at around 664 °C, which was in good agreement with the calculation results in Fig. 1a. Considering the melting point of the outer aluminum can, the final semisolid extrusion temperature was set to be 645 °C. At this temperature, the mass fraction of liquid phase in Al-8030 is approximately 18.5 wt%.

The preparation process is divided into four parts: Al-8030 powder modification, ball-less wet mixing, pyrolysis removal of modifier and semisolid extrusion. The corresponding experiment details are specified as follows:

1. Al-8030 powder modification: The solution of 3 wt% PVA and deionized water were first slowly poured into the slurry of 8030 alloy powder and deionized water and stirred well magnetically. After stirring for 20 min, the steps of vacuum filtration and washing were repeated to obtain the PVA-coated Al-8030 powder.

2. Ball-less wet mixing: GNPs previously ultrasonically dispersed in anhydrous ethanol for 30 min were slowly poured into PVA-coated Al-8030
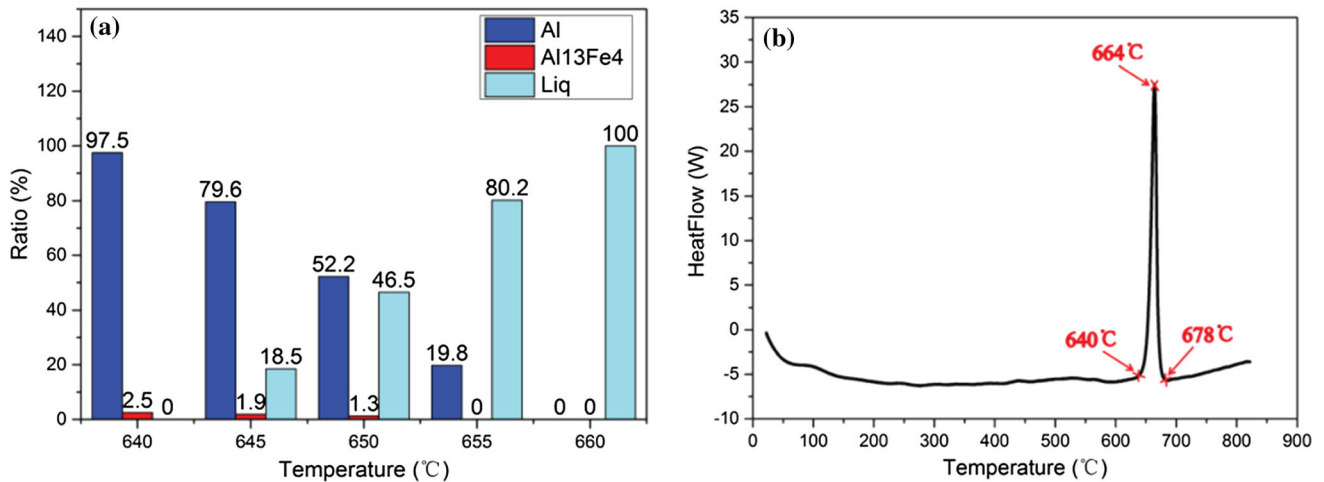
Figure 1 **a** Calculated solid–liquid ratio of 8030 alloy powder, **b** DTA curve of 8030 alloy powder from room temperature to 850 °C.

anhydrous ethanol slurry under magnetic stirring and then transferred to a stainless steel tank and mixed at 200 rpm for 5 h on a biaxial mixer. The mixed slurry was then transferred to a vacuum oven for thorough drying at 100 °C for about 8 h.

3. Pyrolysis removal of modifier: The dried GNPs/Al-8030 mixed powder was heated in a tube furnace at 300 °C for 1.5 h under a flowing argon atmosphere to remove PVA. The mixed powder after removing the PVA was placed in a pure aluminum can (φ50 × 93 mm) and then compacted and tightly sealed to obtain an extruded blank in an argon-protected glove box.

4. Semisolid extrusion: The prepared aluminum-clad-protected billet was heated to 645 °C for 1 h, and the mold was also heated to 530 °C for 1 h, and semisolid extrusion was performed on a 300 t vertical extruder at an extrusion ratio of 36:1 to obtain a φ10 mm extrusion rod. The extruded rod was peeled off the surface to obtain a rod of φ8 mm and then subjected to stress-relieving annealing at 300 °C for 2 h to obtain the final GNPs/Al-8030 composite sample.

The reference samples (Al-8030 with 0 wt% GNPs) were prepared by the same process.

Characterization

The conductivity of the samples was tested on the AT512 precision resistance tester with the samples of 1 m in length at room temperature, and the mechanical properties were tested on the 810-MTS with a traction speed of 0.5 mm/min. The microstructure of the samples was characterized using the Nova NanoSEM 230 field emission scanning electron microscope (FESEM) with an electron-dispersive spectroscopy (EDS) and the Tecnai G220 ST transmission electron microscope (TEM) and Rigaku Dmax 2550 X-ray diffractometer (10° ∼ 90°, 4°/min). The relevant properties of GNPs were characterized using Park XE-100 Atomic Force Microscope and LabRAM ARAMIS Micro-laser Raman Spectrometer. The powder size was measured by the MICRO-PLUS laser diffraction particle size analyzer, and differential thermal analysis of Al-8030 powder was performed on a SETSYS 18/24 integrated thermal analyzer with a 5 °C/min ramp rate.

Results and discussion

Microstructure

The structure and morphology analysis results of the original GNPs are shown in Fig. 2. The FESEM image (Fig. 2a) shows that it has a large specific surface area and good light transmission. At the same time, we can also see the folded GNPs and the upturned GNPs, showing its soft characteristics. Figure 2b is an AFM image of GNPs, and Fig. 2d is the corresponding depth profile along the line marked in Fig. 2b. The thickness of GNPs measured in a relatively flat area without multiple overlaps is about 2–3 nm (6–9 layers). The Raman spectra of GNPs (Fig. 2c) show that three typical peaks are roughly at 1350 cm^{-1}, 1580 cm^{-1} and 2670 cm^{-1}, which correspond to the D peak, G peak and 2D peak, respectively. The D peak
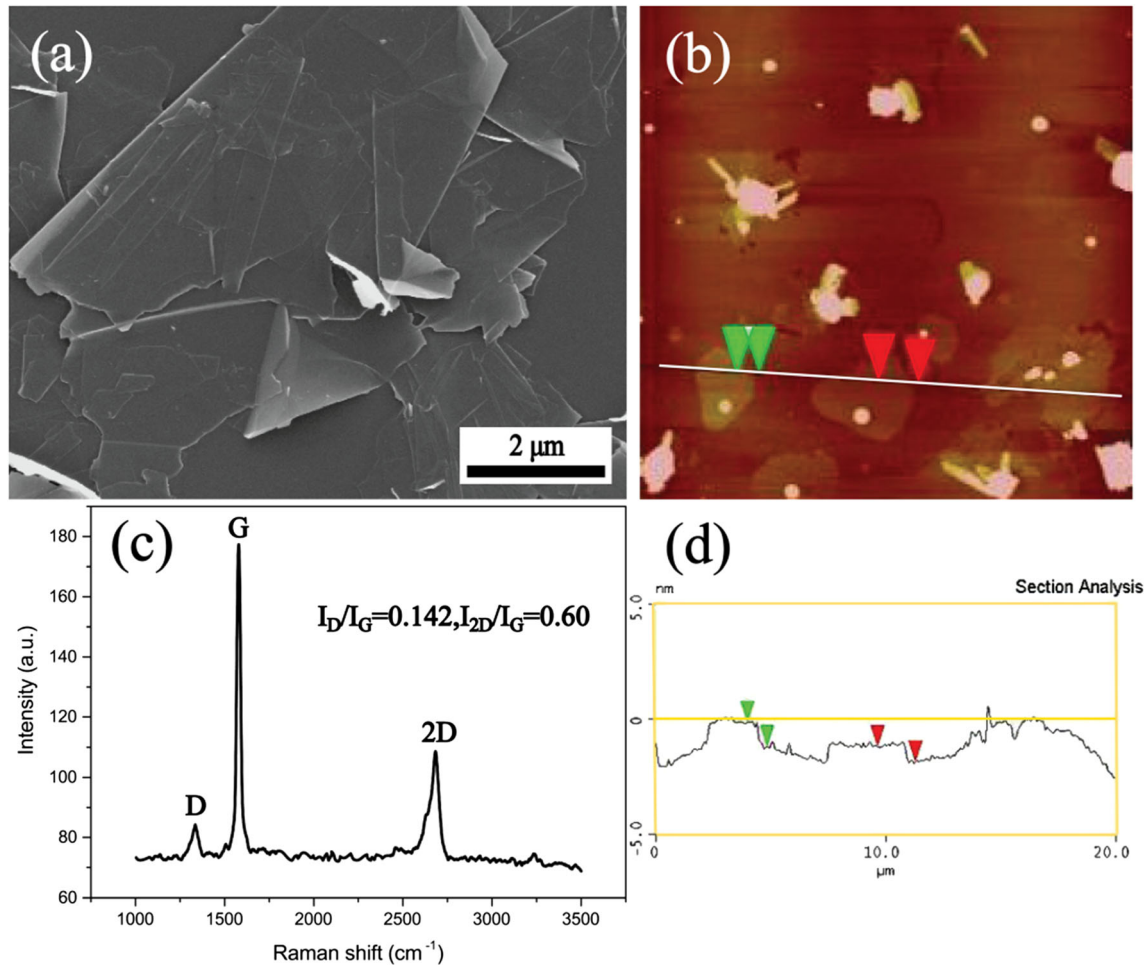
Figure 2 Characterization of original GNPs: **a** FESEM image depicting the morphology of the GNPs; **b** AFM image: the thickness measurement of the GNPs; **c** Raman spectra of the GNPs; **d** the corresponding depth profile along the line marked in (**b**).

is related to the structural defects of GNPs, and the G peak represents the SP^2 structural characteristic peak, reflecting the symmetry and the degree of crystallization, while the 2D peaks represent inelastic scattering from two phonons [21]. Usually, the intensity ratio of D peak to G peak (I_D/I_G) can be employed to evaluate the defect density of GNPs [22, 23], and the intensity ratio of 2D band and G band (I_{2D}/I_G) can be used to estimate the numbers of GNPs layers [24]. In this work, the ratio value of I_D/I_G was only 0.142, and I_{2D}/I_G was 0.60, which means that the original GNPs used in this study are multilayered and have a low defect level. This is consistent with the results of the AFM test.

The FESEM image of the Al-8030 powder in Fig. 3a shows that it has a relatively good sphericity and its average size is around 20 μm, according to the results of powder particle size measurement (Fig. 3b). It is

well known that the surface of aluminum alloy powder is hydrophobic due to the easy formation of an oxide film. This process utilizes PVA to improve the surface hydrophilicity of the Al-8030 powder, and PVA acts as a binder to adhere GNPs to the powder surface. Figure 3c, d shows the morphology of Al-8030 powder and GNPs before and after mixing. It can be clearly seen from Fig. 3d that a layer of GNPS adheres to the surface of Al-8030 powder, which means the improvement of the dispersion of GNPs in the composites.

Figure 4 shows the FESEM of the cross section and longitudinal section of the two samples after semi-solid extrusion. After measuring and averaging in the horizontal, vertical and diagonal directions of the cross-sectional view (Fig. 4a, c), both the grain sizes are about 6 μm, which indicated that the addition of 0.5 wt% GNPs does not significantly refine the grain
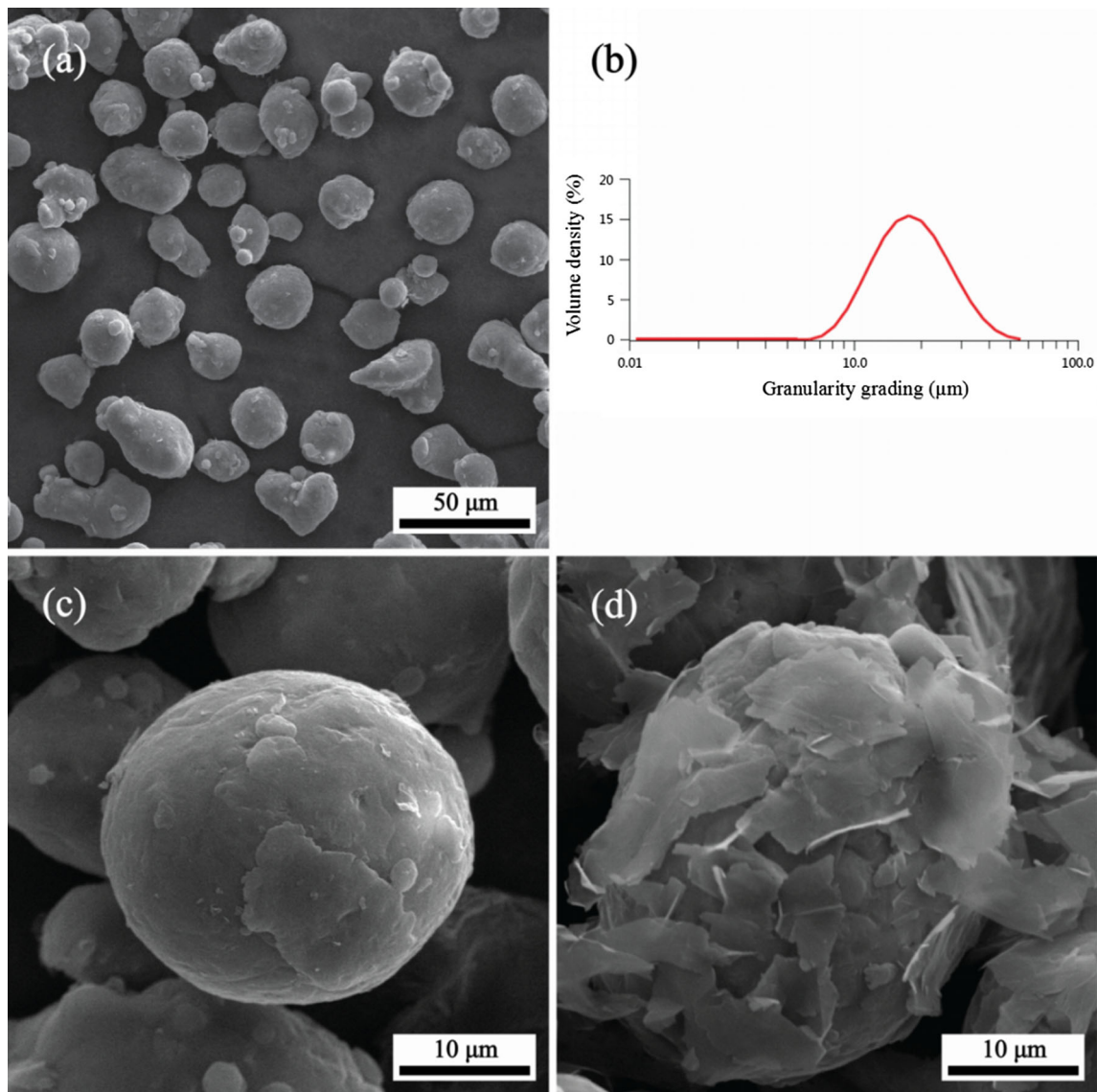
Figure 3 **a** FESEM image of Al-8030 powder; **b** particle size range of Al-8030 powder; **c** Al-8030 powder before mixing; **d** 8030 powder mixed with GNPs.

size. Combining the results of EDS in Fig. 4e, f and the results of XRD in Fig. 5b, it is known that the white contrast is the ($Al_{13}Fe_4$ + Al_2Cu) phase and the black contrast is the GNPs. They are both discontinuously distributed at the grain boundaries on the cross section (Fig. 4a, c) and are parallel to the extrusion direction on the longitudinal section (Fig. 4b, d). This is because during the semisolid extrusion process, the matrix powder is extruded to form a streamlined texture, while the morphology of the GNPs is adjusted to be consistent with the direction of extrusion following the movement of the substrate. It can be clearly seen from the enlarged

details in Fig. 4e, f that the GNPs can be easily bent to adapt to the deformation of the matrix. No pores and micro-cracks are observed at the bonding interface between the GNPs and the matrix, indicating that the GNPs are tightly bound to the matrix.

EPMA map (Fig. 5) of carbon elements in the cross section and longitudinal section of the sample was added to reflect the distribution of GNPs through carbon elements. Sample from cross section of EPMA map shows that GNPs are mainly wrapped in aluminum particles and distributed in the grain boundary. Sample from longitudinal section of EPMA map shows that GNPs are directionally
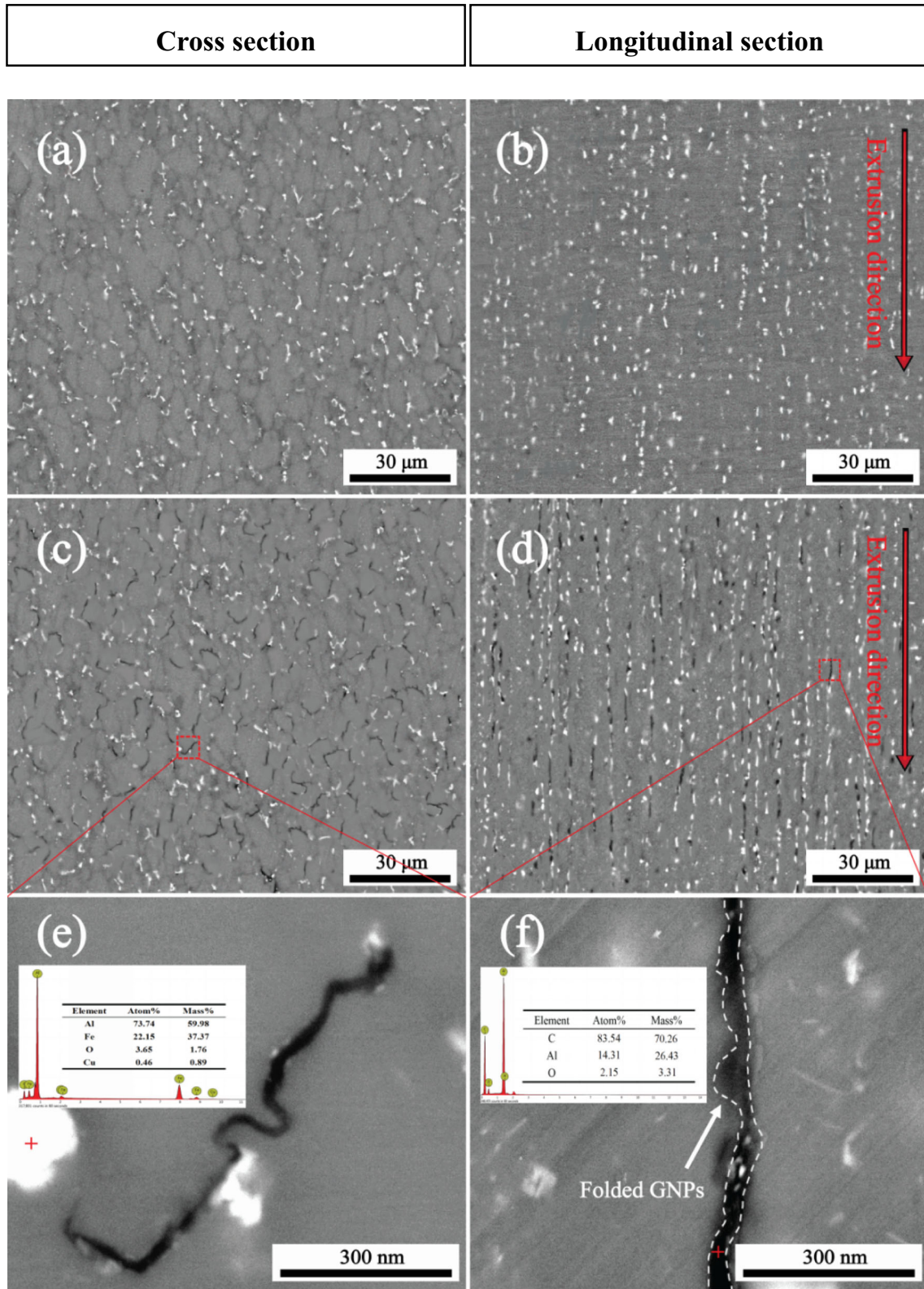
Cross section

Longitudinal section

(a)

(b)

Extrusion direction

30 µm

30 µm

(c)

(d)

Extrusion direction

30 µm

30 µm

(e)

Element	Atom%	Mass%
Al	73.74	59.98
Fe	22.15	37.37
O	3.65	1.76
Cu	0.46	0.89

300 nm

(f)

Element	Atom%	Mass%
C	83.54	70.26
Al	14.31	26.43
O	2.15	3.31

Folded GNPs

300 nm

Figure 4 FESEM images of the samples: **a**, **b** cross section and longitudinal section of the comparative sample; **c**, **d** cross section and longitudinal section of the composite sample (0.5 wt% GNPs/ Al-8030); **e**, **f** enlarged view of the details corresponding to (**c**, **d**) and the results of EDS analysis.
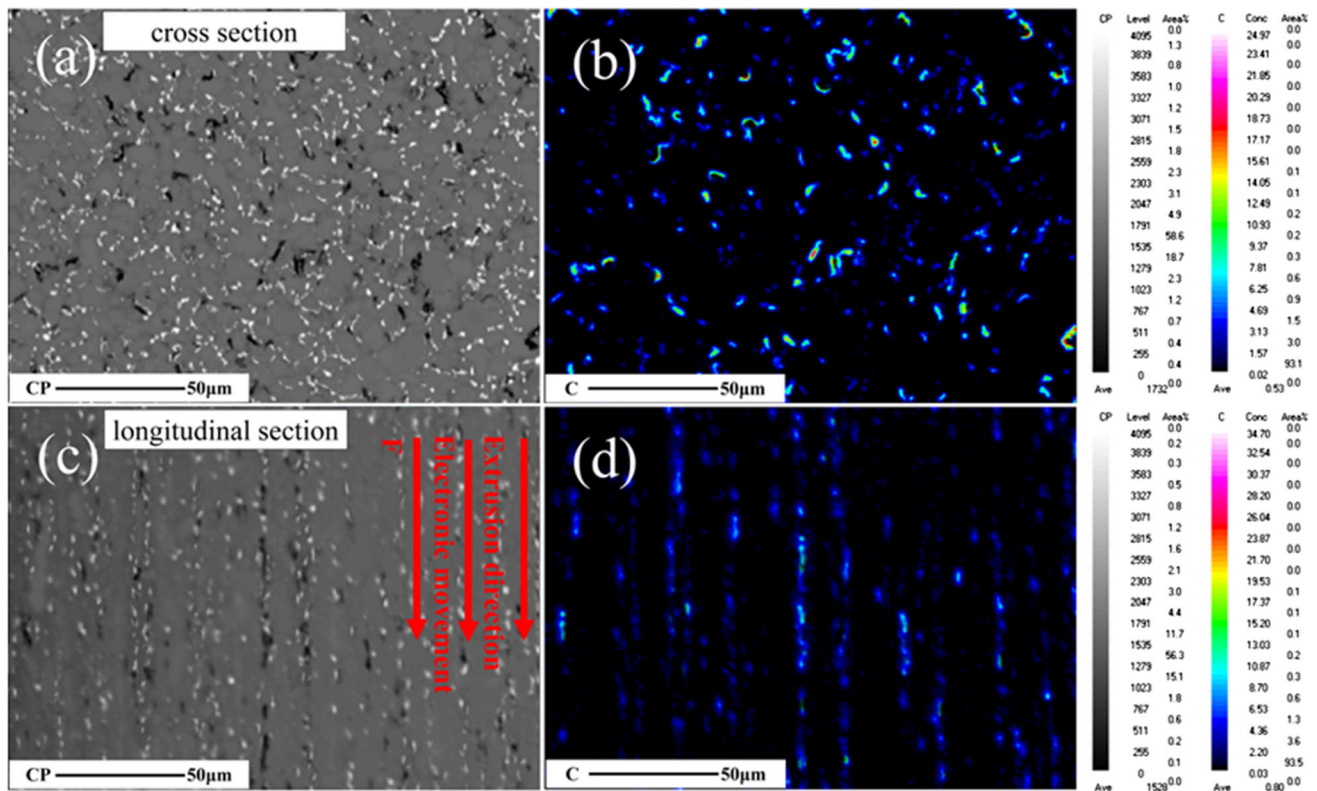
Figure 5 The EPMA image of cross section and longitudinal section of GNPs/Al-8030 composites.

distributed and parallel to the direction of extrusion, the direction of electronic motion and the direction of tensile stress during testing.

Comparing the Raman spectra of GNPs after mixing and semisolid extrusion with the original GNPs (Fig. 6a), it was found that the I_D/I_G values of GNPs were almost unchanged, ranging from 0.142 to 0.143 and 0.143, indicating the structure of GNPs is well protected during the preparation process. Moreover, the I_{2D}/I_G values were also slightly reduced from 0.60 to 0.59 and 0.58, reflecting a low degree of agglomeration of GNPs in the prepared samples. According to the XRD diffraction pattern of the 0.5 wt% GNPs/Al-8030 composites sample (Fig. 6b), it is known that the Al-8030 matrix has a small amount of $Al_{13}Fe_4$ phase and Al_2Cu phase because Fe and Cu elements are hardly dissolved in the Al matrix at room temperature, which is consistent with the results of previous studies [3, 25, 26]. At the same time, no carbides such as Al_4C_3 and FeC_3 were detected, which was attributed to the fact that the preparation process did not introduce too many structural defects into GNPs, so that GNPs were not easily reacted with the matrix at high temperatures [27]. This also means that there

may be no chemical bonding between the GNPs and the substrate. But it should not be ignored that this may be because the carbide content is too small to be detected.

The presence of GNPs in the samples was confirmed, and the interfacial binding of GNPs to the matrix was further observed by TEM. It is observed in Fig. 7a that GNPs still maintain a good stretching posture and a large diameter-to-thickness ratio (GNPs indicated by arrows in the figure), which is advantageous for exerting the enhancement effect of GNPs. The HRTEM images of GNPs in Fig. 7b show a clean interface between GNPs and the matrix, indicating that GNPs do not react with the matrix to form carbides, which confirms the results of XRD detection. From the enlarged details of the interface transition zone between GNPs and matrix in the figure, it can be seen that carbon atoms and aluminum atoms diffuse with each other, indicating that GNPs combine with matrix by diffusion. Similar analysis results were reported by Tian et al. [28] and Bustamante et al. [17]. GNPs that are exposed at the edge of the thin zone are captured in the TEM bright-field image of the longitudinal section (Fig. 7c). The
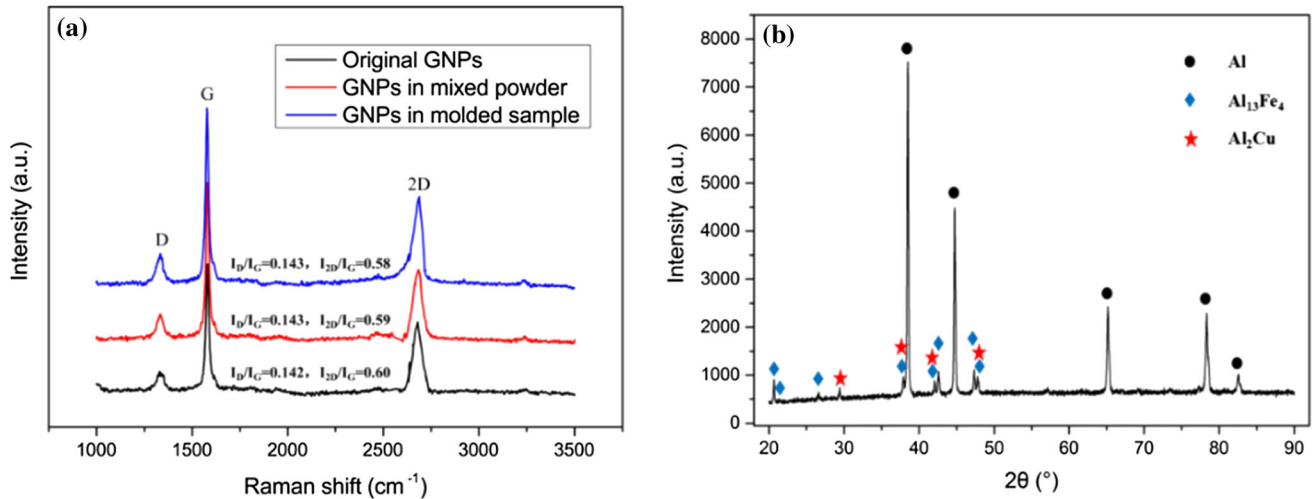
Figure 6 **a** The comparison of Raman spectra of GNPs; **b** XRD diffraction pattern of the 0.5 wt% GNPs/Al-8030 composite sample.

SAED pattern shows several groups of diffraction spots with obvious hexagonal symmetry, demonstrating a multilayer GNPs with a high crystallinity [29]. However, it can be seen that the edges of the GNPs are thicker and multilayered, meaning that there are still a small number of folded or overlapped GNPs, which is consistent with the phenomenon indicated by the arrow in Fig. 4f. This may be because the flexible GNPs are prone to folding in half, as shown in Fig. 2a. Alternatively, when the powder particles are bonded to each other, the GNPs layers are overlapped and are not staggered with deformation.

Relative density and conductive properties

The density and conductivity of the composites and reference samples were tested, and the results are shown in Table 2. As can be seen from the results in Table 2, the samples prepared by this process all have a very high relative density ($\geq 99\%$). This is mainly due to the presence of a part of the liquid phase in the sample during the semisolid extrusion, which is easy to fill the micro-pores and micro-cracks under compression to promote the tight binding of GNPs to the matrix.

At the same time, we found that the composites (with 0.5 wt% GNPs added) still have comparable conductivity compared to the reference sample (only slightly reduced from 62.20 to 61.86%IACS). The classical free electron theory [30] states that lattice vibration, defects, impurity atoms and interfaces would increase the scattering of electrons in the

crystal and thus reduce the conductivity. GNPs have higher conductivity than Al matrix, and their influence on conductivity mainly comes from the blocking of electrons by the bonding interface. According to the microstructure analysis, one of the reasons is that the added GNPs are distributed at the grain boundaries, which reduces the lattice distortion caused by the addition of the second phase, and the second reason is that the distribution of GNPs and precipitates is parallel to the direction of electron motion, greatly reducing the scattering effect of electrons on the phase interface.

Tensile properties

The change in strength caused by the addition of GNPs can be directly reflected by the traditional tensile test. Figure 8 shows the stress–strain curves for the two groups of samples, and the corresponding strength and elongation values for the curves are summarized in Table 3. As can be seen from the tensile test results, after the addition of 0.5 wt% GNPs, the yield strength ($\sigma_{0.2}$) increased from 85.0 to 116.9 MPa with an enhancement rate of 37.5%, while the tensile strength (σ_b) increased from 130.6 to 212.7 MPa with an enhancement rate of 62.9%. At the same time, we found that the elongation of the composites is still comparable to the matrix, only slightly reduced from 23.09 to 22.67%.

In order to facilitate comparison with other research results, we use a strength increment (R) of the composites relative to the matrix to express the enhancement effect by adding a unit volume fraction
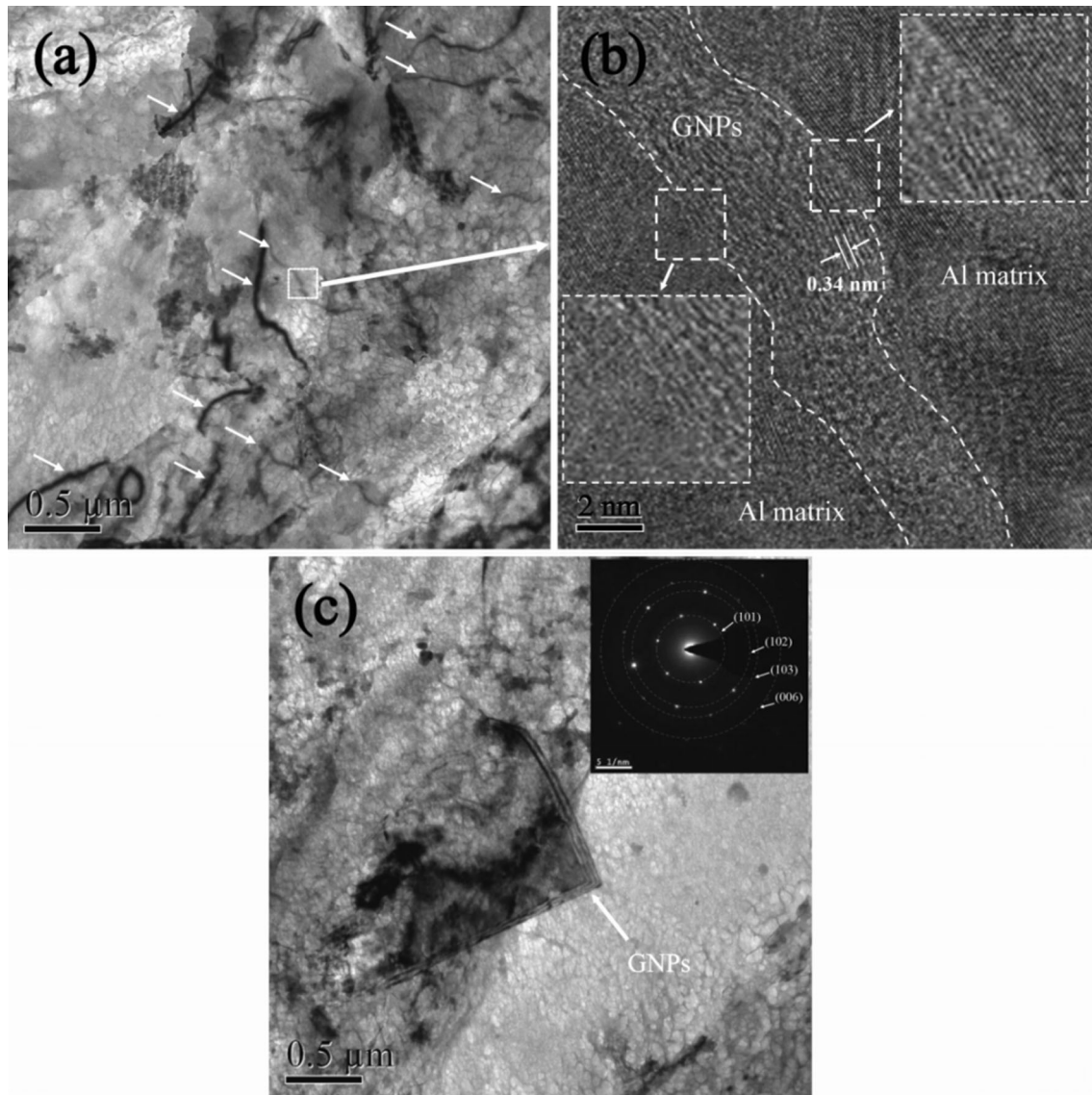
Figure 7 a TEM bright-field image of the cross section of the 0.5 wt% GNPs/Al-8030 composites (GNPs indicated by the arrows); **b** HRTEM image of the GNPs (the boxes in the figure show the interfacial transition zone between GNPs with matrix); **c** TEM bright-field image of longitudinal section of 0.5 wt% GNPs/Al-8030 composites (GNPs exposed at the edge of the thin zone are observed) and selected diffraction pattern of GNPs.

Table 2 Relative density and conductivity of the samples

	Theoretical density (g/cm^3)	Measured density (g/cm^3)	Relative density (%)	Conductivity (IACS%)
Al-8030	2.7495	2.7366 ± 0.0015	99.53	62.20 ± 0.17
0.5 wt%GNPs/Al-8030	2.7453	2.7231 ± 0.0034	99.19	61.86 ± 0.21

of GNPs. This strength increment (R) is defined by the following formula:

$$R = \frac{\sigma_c - \sigma_m}{V_f \cdot \sigma_m} \quad (1)$$

In the formula, σ_c and σ_m are the tensile strengths of the composite and the matrix, respectively, and V_f is the volume fraction of GNPs. According to the results in Table 4, this work achieved a higher efficiency than most of the research results ($R = 96.7$).
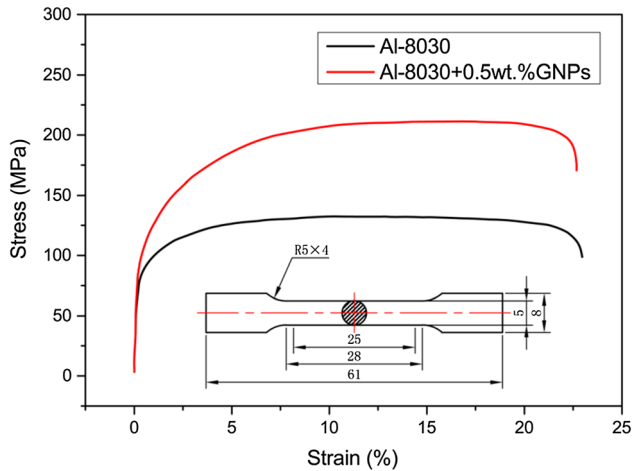
Figure 8 Engineering stress–strain curves of samples at room temperature.

The high strength improvement rate obtained in this experiment is attributed to the distribution of GNPs parallel to the tensile stress direction. Since the degree of plastic deformation of GNPs and Al matrix is inconsistent, shearing occurs at the interface between the two. If the phase angle of GNPs and tensile stress direction is $> 0°$, the force analysis shows that the tensile stress at this time will decompose the component of a vertical GNPs plane, which accelerates the separation of GNPs from the matrix and reduces the interfacial shear strength of both. Therefore, GNPs directional distribution will bring the largest interfacial shear strength in the extrusion direction. However, the value of R is also lower than that in a few studies because GNPs are multilayered and a small number of GNPs are overlapped. However, in combination with the elongation, the composites prepared in this experiment have better comprehensive mechanical properties.

Figure 9 shows the tensile fracture morphology of the two groups of samples. In Fig. 9a, b, we can see a large number of dimples and holes in the fracture of both the samples, but the number of holes in the sample with GNPs added is more. Combined with the elongation data, it is known that the fracture type of the samples belongs to ductile fracture. Typical wavy shear tear lines can be observed on the inner wall of the hole (Fig. 9c), while the extracted GNPs are observed in the holes (Fig. 9d). These characteristics indicate that the interface between GNPs and the matrix undergoes shear fracture during stretching, and the load can be effectively transferred to GNPs. GNPs differ from other reinforcements in that they are a tough phase. It can be seen from Fig. 7a that the flexible GNPs are easily bent, which allows them to moderately stretch under stress to disperse the stress concentration [35, 36]. This is the main reason why composites still maintain a comparable elongation to the matrix.

Strengthening mechanism

One of the reasons some researchers are willing to explain for the increase in strength is that the added graphene reduces the grain size, thus obtaining fine grain strengthening [37, 38]. However, in the microstructure in Fig. 4a, c, no significant grain refinement was observed. This is because the deformation of the grains is not large during the semisolid extrusion process, and the cooling is rapid after the extrusion, so that the degree of grain recovery and recrystallization is low. Therefore, the effect of fine grain strengthening is not obvious in this work.

Second, it can be clearly seen from the fracture morphology in Fig. 9d that the matrix around GNPs has undergone a large degree of deformation, indicating that the deformation degree inside the grain is greater than that at the boundary, and GNPs play a role in hindering dislocation movement. Unlike SiC and carbon nanotubes, graphene has a larger two-dimensional plane and good flexibility, making it more difficult for dislocations to cut through and bypass. Figure 10 shows the TEM bright-field image of the cross section near the fracture of the matrix and composites. It can be seen that it is easier for the dislocation to bypass the fine precipitate phase (Fig. 10a), but it is difficult to bypass the wide GNPs plane (Fig. 10b).

Third, the degree of plastic deformation between GNPs and aluminum alloy matrix was mismatched

Table 3 Tensile strength and elongation values of the samples

Sample	Yield strength (MPa)	Ultimate tensile strength (MPa)	Elongation (%)
Al-8030	85.0 ± 3.5	130.6 ± 5.1	23.09 ± 0.2
0.5 wt%GNPs/Al-8030	116.9 ± 4.9	212.7 ± 7.0	22.67 ± 0.2

Table 4 Mechanical properties and strength increment (R) of graphene/aluminum matrix composites with different contents in different preparation processes

Samples	Preparation process	Tensile strength (MPa)	Strengthening efficiency (R)	Elongation (%)
0.5 wt%GNPs/Al-8030 (this work)	Surface-modified wet mixing + semisolid extrusion	212.7	96.7	22.67
0.3 wt%GNPs/Al [11]	Wet mixing + sintering + hot extrusion	280	28.5	9.53
0.5 wt%GNFs/Al–Mg–Cu [16]	Ball mill wet mixing + hot isostatic pressing + hot extrusion	467	19.5	12
1.0 wt%GNFs/Al [18]	Low-temperature ball milling + hot extrusion	248	54.6	8.3
1.5vot. %GO/Al (flake) [31]	Surface-modified wet mixing + vacuum hot pressing	315.8	38.6	6
0.5 wt%GNPs/Al5083 [32]	Ball mill + hot pressing + hot extrusion	434	68.5	4.6
0.4 wt%GNPs/Al [33]	Wet mixing + SPS sintering + hot extrusion	173	120	16.2
0.4 wt%GNPs/Al [34]	Ball mill + hot extrusion + cold drawing	219	102.1	0.84
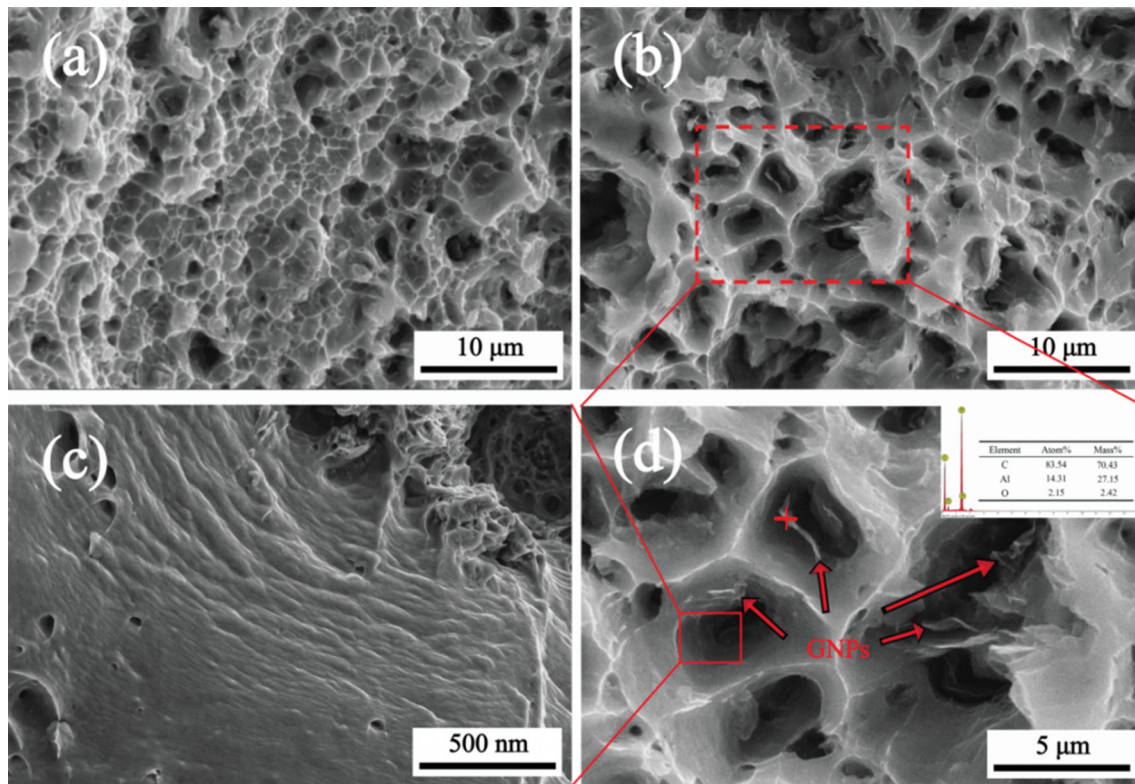
Figure 9 Tensile fracture morphology of samples: **a** Al-8030; **b** 0.5 wt% GNPs/Al-8030 composites; **c** an enlarged view of the typical wavy shear lines on the inner wall of the pit in (**d**); **d** an enlarged view of (**b**) showing the pit detail.

due to the huge difference in Young's modulus between GNPs and aluminum alloy matrix (the Young's modulus of graphene is about 1100 GPa [6], while that of the aluminum alloy matrix is about 72 GPa [39]), and the load was shear-transferred through the bonding interface between GNPs and

matrix. Therefore, the yield strength of the composites (σ_c) could be calculated by the modified shear lag theory [40]:

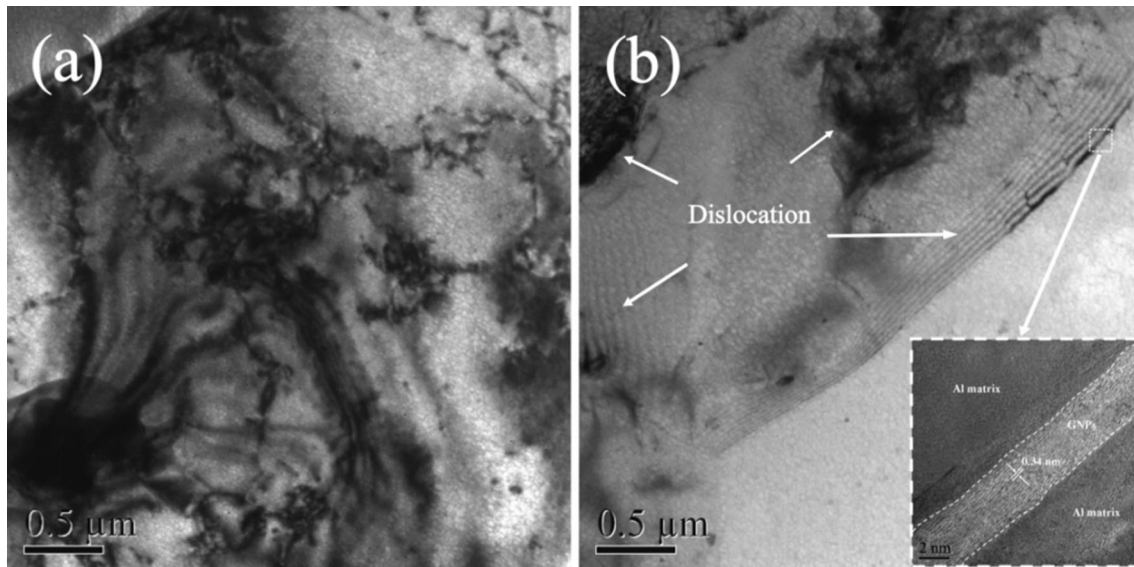$$\sigma_c = \sigma_{ym}\left[1 + \frac{(L+t)A}{4L}\right]f_v + \sigma_{ym}(1 - f_v) \qquad (2)$$

Figure 10 TEM bright-field image of the cross section near the fracture. **a** Matrix; **b** 0.5 wt% GNPs/Al-8030 composite sample.

where σ_{ym} is the yield stress of the Al-8030 matrix, L and t are the lengths of the GNPs parallel and perpendicular to the applied stress, respectively (L = 8.96 µm, t = 3 nm), A is the diameter-to-thickness ratio of GNPs and f_v is the volume fraction of GNPs (f_v = 0.65 vol%). The yield stress value of the matrix (85 MPa) and the relevant parameters of GNPs mentioned above would be used in the calculation. Finally, the calculated strength value of 0.5 wt% GNPs/Al-8030 composites was 497.7 MPa. This value was still greater than the measured value of this work, although a significant increase in yield strength (up to 37.5%) has been achieved. This may be related to the fact that GNPs are not bonded to the matrix by chemical bonding and GNPs are folded or overlapped. In addition, some researchers believed that the soft GNPs plane would be stretched during the plastic deformation [41], which may weaken the shear strength due to the shear asynchronism caused by the extension of the wrinkled structure.

It is also less noticed that the GNPs spaced apart in the matrix (as shown in Fig. 4d, e) not only hindered the dislocation motion, but also shifted the direction of micro-crack propagation. (When the micro-cracks encountered GNPs during the expansion process, shearing separation occurred along the bonding interface between the GNPs and the matrix, and the shear crack can be clearly seen in Fig. 9d.) The non-planar crack that changed the direction of growth had a larger surface area than the plane crack and

needed to absorb more fracture work, thereby compensating for the decrease in toughness caused by the mismatch of plastic deformation degree. Therefore, crack deflection should also be an important reason for the increased strength of this composite while still maintaining considerable toughness.

According to the above analysis, the microscopic process of fracture failure of Al-8030 + 0.5 wt% GNPs composites can be summarized as shown in the schematic diagram in Fig. 11: Under tensile stress, the GNPs distributed at the grain boundary hindered the dislocation propagation, resulting in stress concentration. The micro-cracks were preferentially generated from the weak interface between the GNPs and the matrix and were separated under continuous shear. Then, the crack propagated into the grain and deflected when it encountered the next piece of GNPs. Finally, the crack gradually extended until it breaks.

Conclusions

The mechanical properties and electrical conductivity of 0.5 wt% GNPs/Al-8030 composites prepared by powder modification + semisolid extrusion were investigated. A significant result is that the yield strength and tensile strength of the 8030 aluminum alloy are increased by 37.5% and 62.9%, respectively, while the plasticity and electrical conductivity remain comparable to the matrix. This is due to the fact that
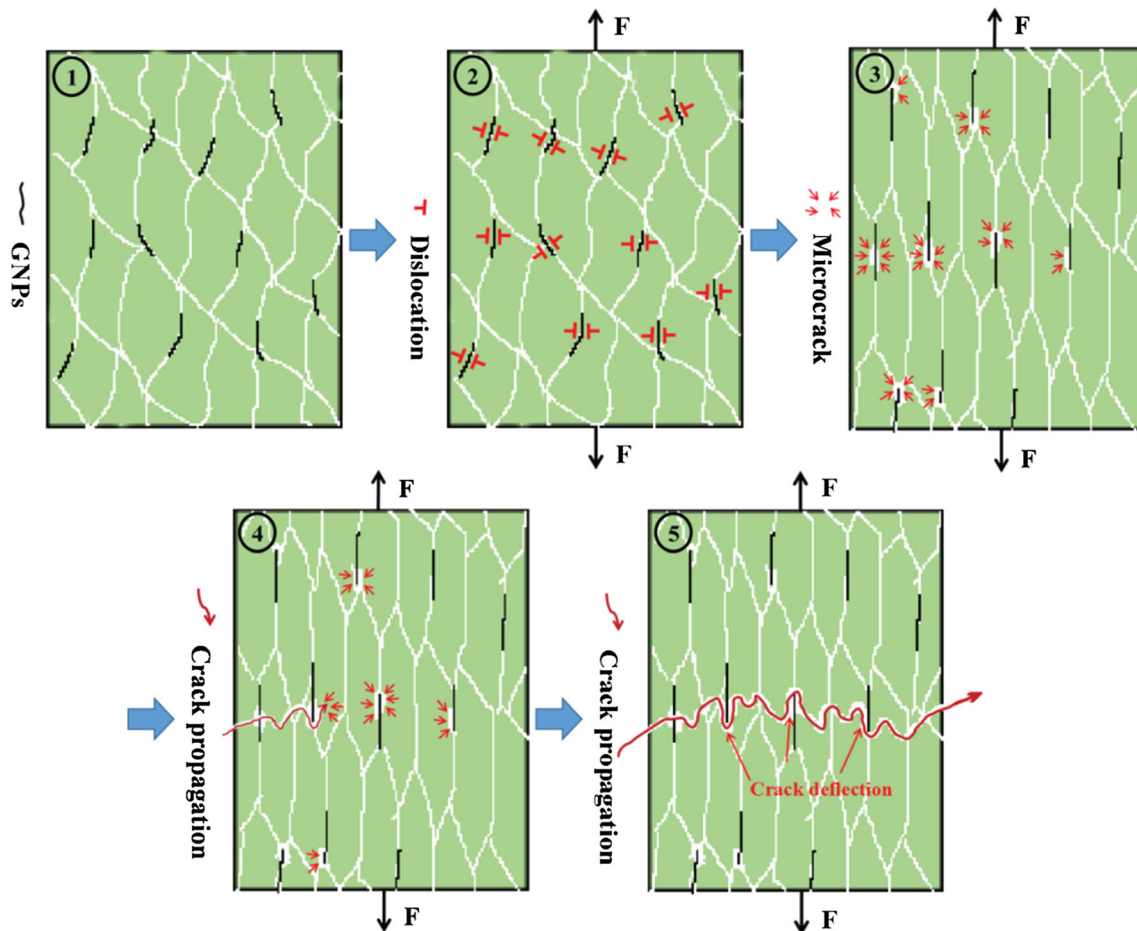
Figure 11 Schematic diagram of microscopic process of fracture failure of 0.5 wt% GNPs/Al-8030 composite.

the preparation process fully protects the structural integrity of the GNPs and the good bonding interface between the GNPs and the matrix, so that the GNPs can fully exert the advantages of the large diameter-to-thickness ratio to hinder the dislocation motion and deflect the crack. Second, the directed distribution of GNPs has the least scattering effect on moving electrons and has the largest interfacial shear strength with the matrix. These factors give the composites a better comprehensive performance.

Compliance with ethical standards

Conflict of interest The authors declare that they have no conflict of interest.

References

[1] Kong XX, Zhang H, Ji XK (2014) Microstructures and mechanical properties evolution of an Al–Fe–Cu alloy processed by repetitive continuous extrusion forming. Mater Sci Eng A 612:131–139

[2] Zhang XY, Zhang H, Kong XX, Fu DF (2015) Microstructure and properties of Al–0.70Fe–0.24Cu alloy conductor prepared by horizontal continuous casting and subsequent continuous extrusion forming. Trans Nonferr Met Soc China 25:1763–1769

[3] Zhang JY, Jiang XY, Ma MY, Jiang B, Wang B, Yi DQ (2017) Effect of scandium micro-alloying on the creep resistance properties of Al-0.7 Fe alloy cables. Mater Sci Eng A 699:194–200

[4] Zhang JY, Wang HX, Yi DQ, Wang B, Wang HS (2018) Comparative study of Sc and Er addition on microstructure, mechanical properties, and electrical conductivity of Al-0.2 Zr-based alloy cables. Mater Charact 145:126–134

[5] Geim AK (2009) Graphene: status and prospects. Science 324:1530–1534

[6] Lee CG, Wei XD, Kysar JW, Hone J (2008) Measurement of the elastic properties and intrinsic strength of monolayer graphene. Science 321:385–388

[7] Bolotin KI, Sikes K, Jiang Z, Klima M, Fudenberg G, Hone J, Kim P, Stormer HL (2008) Ultrahigh electron mobility in suspended graphene. Solid State Commun 146:351–355

[8] Balandin AA, Ghosh S, Bao W, Calizo I, Teweldebrhan D, Miao F, Lau CN (2008) Superior thermal conductivity of single-layer graphene. Nano Lett. 8:902–907

[9] Yan SJ, Dai SL, Zhang XY, Yang C, Hong QH, Chen JZ, Lin ZM (2014) Investigating aluminum alloy reinforced by graphene nanoflakes. Mater Sci Eng A 612:440–444

[10] Rashad M, Pan F, Tang A, Asif M (2014) Effect of graphene nanoplatelets addition on mechanical properties of pure aluminum using a semi-powder method. Prog Nat Sci Mater Int 24:101–108

[11] Hwang J, Yoon T, Jin SH, Lee J, Kim TS, Hong SH, Jeon S (2013) Enhanced mechanical properties of graphene/copper nanocomposites using a molecular-level mixing process. Adv Mater 25:6724–6729

[12] Kim JW, Lee TJ, Han SH (2014) Multi-layer graphene/copper composites: preparation using high-ratio differential speed rolling, microstructure and mechanical properties. Carbon 69:55–65

[13] Rashad M, Pan FS, Hu HH, Asif M, Hussain S, She J (2015) Enhanced tensile properties of magnesium composites reinforced with graphene nanoplatelets. Mater Sci Eng A 630:36–44

[14] Du X, Du WB, Wang ZH, Liu K, Li SB (2018) Ultra-high strengthening efficiency of graphene nanoplatelets reinforced magnesium matrix composites. Mater Sci Eng A 711:633–642

[15] Li M, Gao H, Liang J, Gu S, You W, Shu D, Wang J, Sun B (2018) Microstructure evolution and properties of graphene nanoplatelets reinforced aluminum matrix composites. Mater Charact 140:172–178

[16] Li JL, Xiong YC, Wang XD, Yan SJ, Yang C, He WW, Chen JZ, Wang SQ et al (2015) Microstructure and tensile properties of bulk nanostructured aluminum/graphene composites prepared via cryomilling. Mater Sci Eng A 626:400–405

[17] Pérez-Bustamante R, Bolaños-Morales D, Bonilla-Martínez J, Estrada-Guel I, Martínez-Sánchez R (2014) Microstructural and hardness behavior of graphene-nanoplatelets/aluminum composites synthesized by mechanical alloying. J Alloys Compd 615:578–582

[18] Bartolucci SF, Paras J, Rafiee MA, Rafiee J, Lee S, Kapoor D, Koratkar N (2011) Graphene–aluminum nanocomposites. Mater Sci Eng A 528:7933–7937

[19] Stanford-Beale CA, Clyne TW (1989) Extrusion and high-temperature deformation of fibre-reinforced aluminium. Comps Sci Technol 35:121–157

[20] Wang JY, Li ZQ, Fan GL, Pan HH, Chen ZX, Zhang D (2012) Reinforcement with graphene nanosheets in aluminum matrix composites. Scr Mater 66:594–597

[21] Ferrari AC, Meyer JC, Scardaci V, Casiraghi C, Lazzeri M, Mauri F, Piscanec S, Jiang D et al (2006) Raman spectrum of graphene and graphene layers. Phys Rev Lett 97:187401

[22] Yan LP, Tan ZQ, Ji G, Li ZQ, Fan GL, Schryvers D, Shan A, Zhang D (2016) A quantitative method to characterize the Al4C3-formed interfacial reaction: the case study of MWCNT/Al composites. Mater Charact 112:213–218

[23] Poirier D, Gauvin R, Drew RAL (2009) Structural characterization of a mechanically milled carbon nanotube/aluminum mixture. Compos A 40:1482–1489

[24] Chen FY, Ying JM, Wang YF, Du SY, Liu ZP, Huang Q (2016) Effects of graphene content on the microstructure and properties of copper matrix composites. Carbon 96:836–842

[25] Zhang L, Lück R (2003) Phase diagram of the Al–Cu–Fe quasicrystal-forming alloy system. III. Isothermal sections. Z Metallkd 94:108–115

[26] Cenoz I (2010) Influence of metallic die temperature in the solidification of Cu-10% Al-2% Fe alloy. Arch Metall Mater 55:1029–1033

[27] Ci LJ, Ryu ZY, Jin-Phillipp NY, Rühle M (2006) Investigation of the interfacial reaction between multi-walled carbon nanotubes and aluminum. Acta Mater 54:5367–5375

[28] Tian WM, Li SM, Wang B, Chen X, Liu JH, Yu M (2016) Graphene-reinforced aluminum matrix composites prepared by spark plasma sintering. Int J Miner Metall Mater 23:723–729

[29] Wang HB, Maiyalagan T, Wang X (2012) Review on recent progress in nitrogen-doped graphene: synthesis, characterization, and its potential applications. ACS Catal 2:781–794

[30] Gao HY, Wang J, Shu D, Sun BD (2006) Effect of Ag on the aging characteristics of Cu–Fe in situ composites. Scr Mater 54:1931–1935

[31] Su YS, Li Z, Yu Y, Zhao L, Li ZQ, Guo Q, Xiong DB, Zhang D (2018) Composite structural modeling and tensile mechanical behavior of graphene reinforced metal matrix composites. Sci China Mater 61:112–124

[32] Zhang HP, Xu C, Xiao WL, Ameyama K, Ma C (2016) Enhanced mechanical properties of Al5083 alloy with graphene nanoplates prepared by ball milling and hot extrusion. Mater Sci Eng A 658:8–15

[33] Zhou WW, Fan YC, Feng XP, Kikuchi K, Nomura N, Kawasaki A (2018) Creation of individual few-layer graphene incorporated in an aluminum matrix. Compos A 112:168–177

[34] Li JC, Zhang XX, Geng L (2018) Improving graphene distribution and mechanical properties of GNP/Al composites by cold drawing. Mater Des 144:159–168

[35] Ishigami M, Chen JH, Cullen WG, Fuhrer MS, Williams ED (2007) Atomic structure of graphene on SiO_2. Nano Lett 7:1643–1648

[36] Zhu YW, Murali S, Cai WW, Li XS, Suk JW, Potts JR, Ruoff RS (2010) Graphene and graphene oxide: synthesis, properties, and applications. Adv Mater 22:3906–3924

[37] Yuan QH, Zeng XS, Liu Y, Luo L, Wu JB, Wang YC, Zhou GH (2016) Microstructure and mechanical properties of AZ91 alloy reinforced by carbon nanotubes coated with MgO. Carbon 96:843–855

[38] Rashad M, Pan FS, Zhang JY, Asif M (2015) Use of high energy ball milling to study the role of graphene nanoplatelets and carbon nanotubes reinforced magnesium alloy. J Alloys Compd 646:223–232

[39] Noble B, Harris SJ, Dinsdale K (1982) The elastic modulus of aluminium–lithium alloys. J Mater Sci 17:461–468. https://doi.org/10.1007/BF00591481

[40] Jr RMA, Christodoulou L (1991) The role of equiaxed particles on the yield stress of composites. Scr Metall Mater 25:9–14

[41] Chu K, Wang F, Wang XH, Huang DJ (2018) Anisotropic mechanical properties of graphene/copper composites with aligned graphene. Mater Sci Eng A 713:269–277

Publisher's Note Springer Nature remains neutral with regard to jurisdictional claims in published maps and institutional affiliations.